Modeling a 4-port Microwave-Based Biosensor for 3D Models Mapping

Yuwei Li, Olivia Peytral-Rieu, David Dubuc, Katia Grenier

Modeling a 4-port Microwave-Based Biosensor for 3D Models Mapping

Y. Li, O. Peytral-Rieu, D. Dubuc, K. Grenier

LAAS-CNRS. Université de Toulouse, CNRS, UPS, France
{yli, opeytral, dubuc, grenier}@laas.fr

***Abstract* — This paper proposes a mapping system based on a 4-port biosensor, which is designed to analyze subdivisions of 3D biological models by microwave dielectric spectroscopy. An equivalent electrical model suitable for such a multi-port device is established to extract the electrical characteristics of the different sections of the biological entity. This modeling is based on exploiting the symmetry of the structures and applying a common and differential modes approach, which is derived from the measured scattering parameters. This approach has been validated using several algorithms applied in the MATLAB software. The initial experimental evaluation of the 4-port sensor is performed with ethanol solutions of different concentrations. We therefore demonstrate that the developed electrical model can consider electrical subdivisions of the biological entity.**

***Keywords* — microwave, biosensor, multi–port analysis, electrical model, common and differential modes.**

I. Introduction

Microwave dielectric spectroscopy is getting increased attention as it provides powerful tools with intracellular, non-invasive, label-free, and cost-effective features for biological studies. Microwave-based sensors indeed offer the advantages of high sensitivity, rapid response, and the ability to probe complex biological samples and processes. Consequently, significant investigations have laid the foundation for understanding the interaction between electromagnetic fields and biological materials, culminating in the establishment of microwave dielectric spectroscopy [1]. Previous works use RC electrical modeling of biological samples, at the single cell level [2], [3] and with cell suspensions [4], [5]. Recently, a microwave sensor has also been developed for the dielectric characterization of microtissues [6].

3D microtissues, also called spheroids and even organoids when exhibiting advanced composition close to the physiological complexity of the *in vivo* tissues, are widely used for *in vitro* biomedical research. They indeed closely mimic the realistic cellular microenvironment found in tissues and organs, limiting consequently *in vivo* experiments. So far, traditional equipment employed to analyse such bio-models are based on optical ones. The microwave technology can therefore provide a complementary characterization technique based on the dielectric properties. Its previously listed advantages make it suitable for various applications, with further insights for drug testing, physiological functions for instance. However existing microwave sensors and associated electrical models are designed to operate with 2-port structures, which is incompatible with mapping modifications, limiting and even hindering a comprehensive understanding of complex biological systems.

This paper therefore introduces a four-port sensor configuration aiming to analyze a 3D entity, while considering not only its global dielectric response but also focusing on specific parts of this entity. The first stage toward the mapping of such a 3D and complex structure consists to consider it as divided in four parts. It implies developing an electrical model tailored specifically for the 4-port microwave-based biosensor. The architecture for the 4-port biosensor as well as the microfluidic part is illustrated in section II. The next section is then dedicated to the electrical model specifically developed for such a structure. To validate this electrical model, a mathematical verification is then performed. Finally, preliminary experiments with different concentrations of ethanol are evaluated in section IV.

II. Architecture of the Four-port Biosensor and Its RF Measurement Test Setup

Similar to previously developed 2-port coplanar sensors [3], [5], [7], the four-port device includes a metallic part for the propagation of electromagnetic waves and a fluidic part for handling and maintaining biological samples in liquid, in particular the living cell culture medium.

The four-port biosensor, as depicted in Fig. 1(a), comprises four coplanar waveguides, which exhibit a 10µm wide capacitive gap at the center of the structure for sensing. It includes twice two coplanar accesses implemented with air bridges between grounds to ensure an identical ground level to all four ports. A microfluidic channel (cf. Fig. 1(b)) is placed on the top of the sensor and includes a hydrodynamic trap, which enables the precise location of the 3D model to be dielectrically characterized [7]. Fig. 1(c) presents the cross-section view of the structure at this exact location. The yellow and green layers represent the coplanar waveguides and the fluidic channel material respectively. A three-opened hole configuration in the fluidic channel enables the trapping of the 3D entity and ensures a fluidic flow, which is necessary to keep any biological model in its appropriate host medium.

For microwave characterization, the device under test is connected to a Vector Network Analyzer (VNA C420 from Copper Mountain® Technologies) using two differential coplanar probes and four coaxial cables, whereas measurements are performed from 200 MHz to 3 GHz. A standard short-open-load-through (SOLT) calibration is applied to locate the microwave reference planes at the tips of the RF probes.

An electrical model is then developed to enable considering subdivisions of the 3D entity.

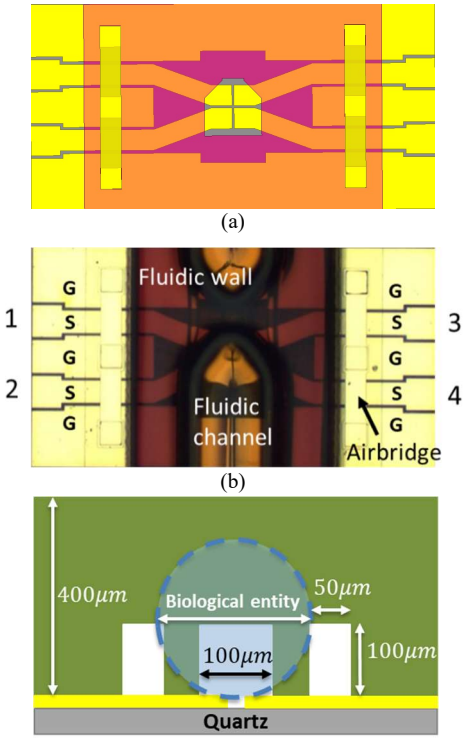

Fig. 1. Four-port biosensor with its microfluidic channel. (a) Schematic of the structure with only the metal and isolation layers. (b) Its photography, where *S* and *G* represent the Signal and Ground strips of the coplanar configuration respectively. (c) Cross-section schematic of the trapping area. The coplanar waveguide is in yellow, whereas the fluidic channel is mentioned in green.

III. Mapping and Electrical Model

Due to the configuration of the considered 4-port microwave biosensor, we have defined an equivalent electrical model, which is given in Fig. 2. The coplanar waveguide accesses are treated as a transmission line, featuring a characteristic impedance of 50 Ω (Z_0). As a first approach, the electrical phase is equal to 0 ($\theta = 0°$) under normalized condition. Y_1 and Y_1' denote the admittances of the microfluidic channel for inflow and outflow respectively, meaning before the trap for Y_1 and with and after the trap for Y_1'. We assume that $Y_1' = Y_1 + \Delta Y$. Thanks to the 4-port system, the biological object, which is located just before the location of the trap, can be modeled with two types of admittances, Y_{2a} and Y_{2b} which are each considered as a capacitance *C* and a conductance *G* in parallel.

Taking the 4-port microwave configuration shown in Fig. 1 into account and its vertical symmetry with a symmetry line located in the middle of the fluidic channel, a differential modeling approach is applied. The differential mode circuit, the *D*-mode, is virtually grounded along the line of symmetry, while the common mode circuit, *C*-mode, is virtually opened.

First, the four-port S parameters are translated from the classical formulas [8] into common (open circuit) and differential (short circuit) modes [9]-[11]. The four physical ports can be viewed as having one input and one output ports associated with a differential signal, or the two ports associated with a common mode signal. Thus, the 4x4 standard *S*-matrix can be transformed into the mixed S_{MN} matrix (cf. Eq. (1)) [12].

$$S_{MN} = \begin{bmatrix} S_{DD} & S_{DC} \\ S_{CD} & S_{CC} \end{bmatrix} \quad (1)$$

The common and differential modes matrices can be expressed as in Eq. (2) and (3), where *C* and *D* correspond to the common and differential modes respectively.

$$S_{CC} = \begin{bmatrix} (s_{11}+s_{13}+s_{31}+s_{33}) & (s_{12}+s_{14}+s_{32}+s_{34}) \\ (s_{21}+s_{23}+s_{41}+s_{43}) & (s_{22}+s_{24}+s_{42}+s_{44}) \end{bmatrix} \quad (2)$$

$$S_{DD} = \begin{bmatrix} (s_{11}-s_{13}-s_{31}+s_{33}) & (s_{12}-s_{14}-s_{32}+s_{34}) \\ (s_{21}-s_{23}-s_{41}+s_{43}) & (s_{22}-s_{24}-s_{42}+s_{44}) \end{bmatrix} \quad (3)$$

In S_{MN} matrix, S_{CC11} corresponds to the common-mode return loss at the common port 1. S_{DD12} is the common insertion loss from the common port 2 to the common port 1. The remaining *S*-parameters are defined similarly, with *DC* corresponding to the differential to common-mode conversion, *CD* corresponding to the common to differential-mode conversion, and *DD* corresponding to differential to differential -mode parameters.

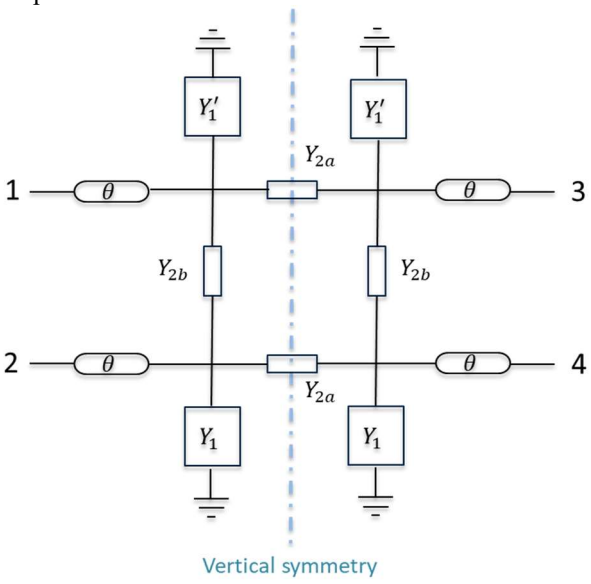

Fig. 2. The equivalent electrical model of the 4-port device. Y_1 and Y_1' denote the admittances of the microfluidic channel.

Due to the symmetrical properties, calculations are carried out considering only one part of the symmetry, leading to two 2-port models. The common and differential modes are illustrated in Fig. 3(a) and Fig. 3(b).

Based on the 2-port system [6], we can obtain S_{CC} parameters as shown below:

$$S_{CC11} = \frac{1-y_1(y_1+2y_{2b})+\Delta y(1-y_1-y_{2b})}{1+y_1(2+y_1+2y_{2b})+\Delta y(1+y_1+y_{2b})+2y_{2b}} \quad (4)$$

$$S_{CC12} = S_{CC21} = \frac{2y_{2b}}{1+y_1(2+y_1+2y_{2b})+\Delta y(1+y_1+y_{2b})+2y_{2b}} \quad (5)$$

$$S_{CC22} = \frac{(1+y_1-y_1')-y_1y_1'-y_{2b}(y_1+y_1')}{(1+y_1+y_1')+y_1y_1'+y_{2b}(2+y_1+y_1')} \quad (6)$$

where $y_x = Y_x \cdot Z_0$.

From the theoretical formula in [8], y_{2b_CC} and Δy_CC can be expressed as given in Eq. (7) and (8):

$$y_{2b\_CC} = \frac{2S_{CC21}}{(1+S_{CC11})(1+S_{CC22})-S_{CC12}S_{CC21}} \quad (7)$$

$$\Delta y\_CC = \frac{2(S_{CC11}-S_{CC22})}{(1+S_{CC11})(1+S_{CC22})-S_{CC12}S_{CC21}} \ . \quad (8)$$

Thus, y_{1_CC} can be calculated as:

$$y_{1\_CC} = \frac{(1-S_{CC11})(1+S_{CC22})+S_{CC12}S_{CC21}-2S_{CC21}}{(1+S_{CC11})(1+S_{CC22})-S_{CC12}S_{CC21}} . \quad (9)$$

Eq. (7), Eq. (8) and Eq. (9) correspond to normalized admittances of the structure when $\theta = 0°$. The CPW accesses located on each side of the device are also considered by adding four transmission lines, exhibiting a characteristic impedance Z_0. The measured *S* parameters become then:

$$\begin{aligned} S'_{CC11} &= S_{CC11}e^{-2j\theta} \quad S'_{CC12} = S_{CC12}e^{-2j\theta} \\ S'_{CC21} &= S_{CC21}e^{-2j\theta} \quad S'_{CC22} = S_{CC22}e^{-2j\theta} \end{aligned} \quad (10)$$

where j is the complex operator, $e^{2j\theta} = {}^{1}/_{S'_{CC11empty}}$ (the "empty" configuration regarding to the *S* parameter when the device is filled with air). By applying the measured *S* parameters to Eq. (7) – (9), the admittances in *C* mode can be obtained as:

$$y_{2b\_CC} = \frac{2\frac{S'_{CC21}}{S'_{CC11empty}}}{\left(1+\frac{S'_{CC11}}{S'_{CC11empty}}\right)\left(1+\frac{S'_{CC22}}{S'_{CC11empty}}\right)-\frac{S'_{CC12}S'_{CC21}}{S'^{2}_{CC11empty}}} \quad (11)$$

$$\Delta y\_CC = \frac{2\left(\frac{S'_{CC11}}{S'_{CC11empty}}-\frac{S'_{CC22}}{S'_{CC11empty}}\right)}{\left(1+\frac{S'_{CC11}}{S'_{CC11empty}}\right)\left(1+\frac{S'_{CC22}}{S'_{CC11empty}}\right)-\frac{S'_{CC12}S'_{CC21}}{S'^{2}_{CC11empty}}} \quad (12)$$

$$y_{1\_CC} = \frac{\left(1-\frac{S'_{CC11}}{S'_{CC11empty}}\right)\left(1+\frac{S'_{CC22}}{S'_{CC11empty}}\right)+\frac{S'_{CC12}S'_{CC21}}{S'^{2}_{CC11empty}}-2\frac{S'_{CC21}}{S'_{CC11empty}}}{\left(1+\frac{S'_{CC11}}{S'_{CC11empty}}\right)\left(1+\frac{S'_{CC22}}{S'_{CC11empty}}\right)-\frac{S'_{CC12}S'_{CC21}}{S'^{2}_{CC11empty}}} . \quad (13)$$

The admittances in *D* mode can be calculated using the method applied to the *C* mode. By comparing the *D* and *C* mode circuits, we can obtain y_{2a} with Eq. (14):

$$y_{2a} = \frac{y_{t\_DD}-y_{1\_CC}}{2} \ , \quad (14)$$

where y_{t_DD} comprises y_1 and $2y_{2a}$ in parallel.

Afterwards, the capacitance *C* and conductance *G* of the targeted entity can be extracted with Eq. (15) and Eq. (16), respectively, where y_x is dedicated to the admittances of the biological entity, i.e. y_{2a} and y_{2b}.

$$C = \frac{1}{2\pi f}\frac{Img(y_x)}{50} \quad (15)$$

$$G = \frac{Re(y_x)}{50} \quad (16)$$

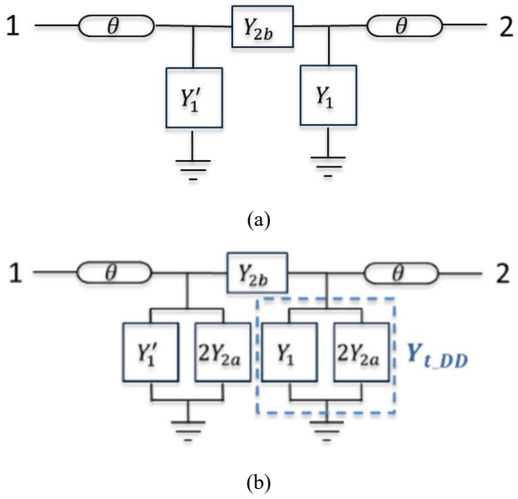

Fig. 3: (a) Common and (b) Differential modes (with $Y'_1 = Y_1 + \Delta Y$).

IV. Equations Validation

The validation of the approach is performed in two steps.

A. Validation of the C and D Modes

In our validation process, we employ a dual-check mechanism. In the first approach, we set Y_x parameters and use derived equations to calculate the *C* and *D* matrices. From these matrices, y_x values are computed using assumed data. A comparison with the initially set of Y_x data ensures consistency. Similarly, in the second approach we assume the *C* and *D* matrices, obtain the Y_x values, and finally infer the corresponding *C* and *D* matrices. This dual-validation strategy provides a robust means of ensuring the accuracy of the method that we proposed by cross-verifying the results obtained through different paths. This procedure is done with MATLAB software.

B. Validation with the Raw S-parameters

In terms of the theoretical four-fold symmetry, the following equivalences given in Eq. (17) are considered for our validation.

$$\begin{cases} S_{11} \equiv S_{22} \equiv S_{33} \equiv S_{44} \\ S_{12} \equiv S_{21} \equiv S_{34} \equiv S_{43} \\ S_{13} \equiv S_{31} \equiv S_{24} \equiv S_{42} \\ S_{14} \equiv S_{41} \equiv S_{23} \equiv S_{32} \end{cases} \quad (17)$$

Using the same methodology as previously described, we first assume the values of the raw *S*-parameter by applying the Eq. (17). Then we obtain the matrices for *C* and *D*, thereby acquiring the y_x values. From the previous equations, we then once again get *C* and *D* matrices. This procedure is indicated in Fig. 4.

We test 20 values for both validations in a range of (0 - 20) for Y_x and (-1 - +1) for *S* parameters to the MATLAB calculation. No difference between the initial items and what we obtain theoretically is found, which validates our calculations.

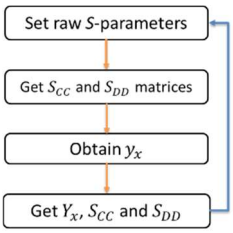

Fig. 4: Validation process with programs applied in MATLAB software

V. Experimental Evaluation of the Sensor and Electrical Model with Ethanol Solutions at Different Concentrations

Before being able to use the sensor with complex biological elements, tests of simpler solutions have been performed with ethanol solutions. Our initial sensitivity analysis of the 4-port mapping sensor involves three ethanol dilutions in DI water with varying concentrations: 10%, 20% and 40%. Deionized water (DI water) is initially measured and referred as 0% ethanol.

Fig. 5 present the example of the capacitance and conductance of y_{2a} obtained for different ethanol solutions. The measurement of each concentration is replicated 4 times. As shown in Fig. 5, the largest value of capacitance is reached with the lowest concentration of ethanol, which is consistent with the theory [13]. Furthermore, both capacitance and conductance exhibit a gradient variation in agreement with the concentration of ethanol.

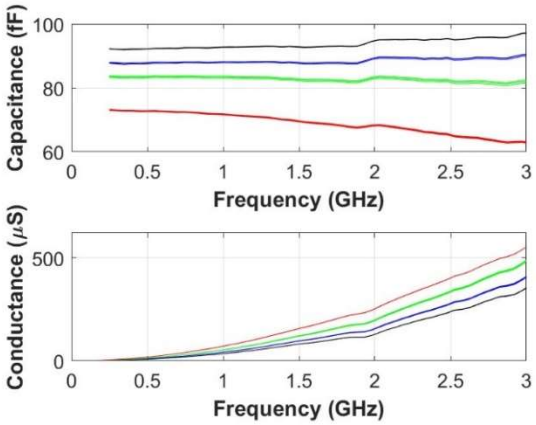

Fig. 5: Capacitance and conductance of different concentrations of ethanol mixed with DI water for y_{2a}. Black: 0%; Blue: 10%; Green: 20%; Red: 40%.

VI. Conclusion

A 4-port biosensor configuration and its electrical modeling is established to enable the mapping of a biological entity. Based on a common and differential modes approach and the symmetry of the structure, the equivalent electrical model can be simplified as a 2-port system, leading to the extraction of the electrical response of a biological entity. In order to verify the proposed electrical model, we checked it through three validations systems based on the criteria initially set. The final section involves the very first experimental evaluation of the sensor with ethanol solutions of different concentrations. Both capacitance and conductance exhibit a gradient variation with the ethanol solutions. Next steps will include more and more complex elements to be characterized, leading to 3D biological models such as spheroids. This multi-port model opens attractive perspectives towards the analyses of complex and heterogeneous biological models.

Acknowledgment

The work was partially supported by the LAAS-CNRS micro and nanotechnologies platform of the French RENATECH network.

References

[1] H. P. Schwan, "Electrical properties of blood and its constituents: alternating current spectroscopy," *Blut,* vol. 46, pp. 185–197, Apr. 1983.

[2] T. Chen, D. Dubuc, M. Poupot, J-J. Fournié, K. Grenier, "Microwave biosensor dedicated to the dielectric spectroscopy of a single alive biological cell in its culture medium," *IEEE International Microwave Symposium*, Seattle, USA, Jun. 2013.

[3] A. Tamra, A. Zedek, M.P. Rols, D. Dubuc, K. Grenier, "Single cell microwave biosensor for monitoring cellular response to electrochemotherapy," *IEEE Trans. on BioMedical Engineering*, vol. 69, pp. 3407–3414, Apr. 2022.

[4] D. J. Currie, M. h. Lee and R. W. Todd, "Prediction of physical properties of yeast cell suspensions using dielectric spectroscopy," IEEE Conference on Electrical Insulation and Dielectric Phenomena, Kansas City, MO, USA, 2006, pp. 672-675.

[5] K. Grenier, D. Dubuc, P-E. Poleni, M. Kumemura, H. Toshiyoshi, T. Fujii, H. Fujita, "Integrated Broadband Microwave and Microfluidic Sensor dedicated to Bioengineering," *IEEE Trans. on Microwave Theory and Techniques*, Vol. 57, pp. 3246-3253, Dec. 2009.

[6] O. Peytral-Rieu, K. Grenier and D. Dubuc, "Microwave Sensor Dedicated to the Determination of the Dielectric Properties of 3D Biological Models from 500MHz to 20GHz," *IEEE MTT-S International Microwave Symposium (IMS)*, Atlanta, GA, USA, 2021, pp. 222-225.

[7] O. Peytral-Rieu, D. Dubuc, K. Grenier, "Microwave-based Sensor for the Non-invasive and Real Time Analysis of 3D Biological Microtissues: Microfluidic Improvement and Sensitivity Study," *IEEE Trans. on Microwave Theory and Techniques*, vol. 71, pp. 4996-5003, Nov. 2023.

[8] D. M. Pozar, Microwave engineering, 4th ed., New York: John Wiley & Sons, 2012.

[9] M. Roberg and C. Campbell, "A Novel Even & Odd-Mode Symmetric Circuit Decomposition Method," *IEEE Compound Semiconductor Integrated Circuit Symposium (CSICS)*, Monterey, CA, USA, 2013, pp. 1-4.

[10] D. E. Bockelman and W. R. Eisenstadt, "Combined differential and common-mode scattering parameters: theory and simulation," *IEEE Transactions on Microwave Theory and Techniques*, vol. 43, pp. 1530-1539, Jul. 1995

[11] J. Reed and G. J. Wheeler, "A Method of Analysis of Symmetrical Four-Port Networks," *IRE Transactions on Microwave Theory and Techniques*, vol. 4, pp. 246-252, Oct. 1956.

[12] K. M. Ho, K. Vaz and M. Caggiano, "Scattering parameter characterization of differential four-port networks using a two-port vector network analyzer," in *Proceedings Electronic Components and Technology. ECTC*'05, Lake Buena Vista, FL, USA, 2005, pp. 1846-1853.

[13] A. H. Sihvola, "Electromagnetic mixing formulas and applications," *IEE Electromagn. Waves Ser.*, vol. 47, pp. 63-68, Jun. 1999.